Annals of Nuclear Energy 94 (2016) 175–188

Contents lists available at ScienceDirect

Annals of Nuclear Energy

journal homepage: www.elsevier.com/locate/anucene

Analysis of ASTEC-Na capabilities for simulating a loss of flow CABRI experiment

A. Flores y Flores [a], V. Matuzas [a], S. Perez-Martin [b], G. Bandini [c], S. Ederli [c], L. Ammirabile [a,*], W. Pfrang [b]

[a] European Commission Joint Research Centre (JRC), Institute for Energy and Transport, Westerduinweg 3, 1755LE Petten, The Netherlands
[b] Karlsruhe Institute of Technology (KIT), Institute for Neutron Physics and Reactor Technology, Hermann-von-Helmholtz-Platz 1, 76344 Eggenstein-Leopoldshafen, Germany
[c] Italian Agency for New Technologies, Energy and Sustainable Economic Development (ENEA), Via Martiri di Monte Sole, 4, 40129 Bologna, Italy

ARTICLE INFO

Article history:
Received 20 November 2015
Received in revised form 26 February 2016
Accepted 27 February 2016
Available online 16 March 2016

Keywords:
CABRI programmes
ASTEC-Na
SIMMER-III
SAS-SFR
Severe accidents
Code benchmarking

ABSTRACT

This paper presents simulation results of the CABRI BI1 test using the code ASTEC-Na, currently under development, as well as a comparison of the results with available experimental data. The EU-JASMIN project (7th FP of EURATOM) centres on the development and validation of the new severe accident analysis code ASTEC-Na (Accident Source Term Evaluation Code) for sodium-cooled fast reactors whose owner and developer is IRSN. A series of experiments performed in the past (CABRI/SCARABEE experiments) and new experiments to be conducted in the new experimental sodium facility KASOLA have been chosen to validate the developed ASTEC-Na code.

One of the in-pile experiments considered for the validation of ASTEC-Na thermal–hydraulic models is the CABRI BI1 test, a pure loss-of-flow transient using a low burnup MOX fuel pin. The experiment resulted in a channel voiding as a result of the flow coast-down leading to clad melting. Only some fuel melting took place.

Results from the analysis of this test using SIMMER and SAS-SFR codes are also presented in this work to check their suitability for further code benchmarking purposes.

1. Introduction

The aim of this analysis is to verify the CABRI test modelling and to assess ASTEX-Na capabilities to describe sodium single and two-phase behaviour under conditions representative of fast reactor operation characteristics. Within the 7th Euratom Framework Program Collaborative Project Joint Advanced Severe accidents Modelling and Integration for Na-cooled fast neutron reactors (JASMIN), a new European severe accident analysis code for sodium cooled fast reactors, ASTEC-Na, is under development. The current development focuses at the initiating phase of the sodium fast reactor (SFR) severe accident sequence. The ASTEC-Na code aims at providing capabilities to evaluate the consequences of unprotected severe accidents including source term evaluation (Girault et al., 2013).

Several experiments from CABRI and SCARABEE programmes (Papin, 2012) are included in the validation matrix of ASTEC-Na in order to assess the capabilities of the code and the reliability of the results.

The representative BI1 Loss Of Flow (LOF) test conducted in the CABRI reactor has been taken as a reference for the first ASTEC-Na code validation and benchmarking phase.

The BI1 test was a LOF experiment using a mixed oxide test pin irradiated in the PHENIX reactor with a maximum burn-up of 1 at.%. The main objectives of the BI1 experiment were threefold (Augier et al., 1981):

- To reach clad melting after voiding initiation and clad dry out without fuel melting.
- To get experimental results on the behaviour of low burnup pre-irradiated test pin fuel (fission gas behaviour, metallurgical modifications, etc.) in order to have a data base for design and safety applications.
- To get a reference for subsequent experiments to be performed within the CABRI-1 programme.

ASTEC-Na results for BI1 test have been compared with experimental data and with other computational safety codes such as SAS-SFR used by KIT and SIMMER-III used by ENEA and JRC for code benchmarking purposes.

After a brief description of the codes and models in Section 2 and of the CABRI BI1 test in Section 3, code modelling and results

* Corresponding author. Tel.: +31 224 56 5064.
E-mail address: luca.ammirabile@ec.europa.eu (L. Ammirabile).

http://dx.doi.org/10.1016/j.anucene.2016.02.032
0306-4549/

of the ASTEC-Na calculation by ENEA and JRC are presented in comparison with available experimental data in Sections 4 and 5, respectively.

2. Codes

2.1. ASTEC-Na

The ASTEC-Na code is under development and validation in the frame of the JASMIN project of the 7th EU Framework Program. The code is an evolution of the European ASTEC code jointly developed by IRSN and GRS for severe accident analysis in light water reactors (Chatelard et al., 2014).

The scope of the developing ASTEC-Na code is to extend its original capability for severe accident analysis in light water reactors to sodium-cooled fast reactors. One important aspect for a reliable transient and accident analysis is the right evaluation of thermal–hydraulic aspects of the primary and secondary circuits using sodium as coolant. In the preliminary V1 version of the code under development and validation, the thermal–hydraulics in the circuits is calculated by the CESAR module which is coupled to the ICARE module that represents the core structures thermal behaviour and their eventual degradation inside the vessel.

The adaptation of the CESAR module to sodium-cooled fast reactors environment has required not only implementing Na properties in the Material Data Bank of ASTEC, but also an update of all the expressions describing heat and mass fluxes between Na phases and between Na and component/system surfaces (Brillant and Laborde, 2014).

The heat and mass exchanges between liquid and vapour are calculated using the kinetic theory of gases. The model considers two opposing flows at the interphase: the vapour molecules hitting the surface and remaining there (i.e., condensation) and the spontaneous liquid evaporation. If vapour and liquid temperatures are identical and Na pressure is the saturation one, both flows should be equal. Two additional phenomena are considered: Na flashing, when the total pressure is lower than the liquid saturation one (i.e., liquid bulk boiling); and bulk condensation, when the Na vapour pressure is greater than the vapour saturation pressure. Beyond heat transfer associated to mass exchange, a convective mechanism between both Na phases has been also accounted for. This term might be significant in volumes which atmospheres consist dominantly of non-condensable gases. The formulation relies on the Newton's law of cooling where the heat transfer coefficient is estimated as the inverse function of a series coupling the individual thermal resistances of phases: pure conduction for the dispersed phase (i.e., bubbles or droplets) and convection for the continuous one.

Wall-to-fluid heat exchanges largely depend on the Na phase. The phenomena modelled for liquid Na are: convection, nucleate boiling, film boiling, thermal radiation and droplet projection (i.e., heat flux from the droplets emerging from the quench front). Convection and radiation are considered for wall-to-Na vapour heat transfer.

The current version of the ASTEC-Na code is not fully capable to perform simulations of the pin mechanical behaviour beyond fuel pin failure/break-up conditions. The models for fuel pin mechanics are included in ASTEC-Na through RIA module, but it still needs some refinements in order to better take into account the specificity of SFR fuel pin behaviour under representative conditions of SFR transients. Further, models for the simulation of the movement of molten pin materials are not yet implemented.

2.2. SIMMER-III

The SIMMER-code (Tobita et al., 2002) has been developed as mechanistic safety analysis tool for liquid metal cooled reactors with fast neutron spectrum. It can be applied to a wide simulation range from normal operation conditions, via transients and accidents, core melting and core destruction to in-vessel relocation phenomena and post-accident heat removal conditions.

SIMMER-III is a two-dimensional (2D), multi-velocity-field, multi-phase, multi-component, Eulerian, fluid-dynamics code system coupled with a structure model for fuel-pins, hexcans and general structures, and a space-, time- and energy-dependent transport theory neutron dynamics model. An elaborated analytical equation-of-state (EOS) closes the fluid-dynamics conservation equations. Although the 3D version SIMMER-IV is available, the main backbone for analyses is still SIMMER-III.

The SIMMER-III code treats thermal behaviour of the fuel pin in the context of implemented heat transfer models. The latter can be divided in two distinct domains related to fluid-dynamics heat transfer and structural heat transfer.

In the fluid dynamics heat transfer domain, the individual, in SIMMER-III implemented models are:

- Non-equilibrium[1] melting/freezing (M/F) model;
- Non-equilibrium vaporisation/condensation (V/C) model; and
- Equilibrium[2] M/F model.

In the structure heat transfer domain, the implemented models concern:

- Fuel pin heat transfer; and
- Hexcan wall heat transfer.

There are thus, five heat transfer models implemented in the SIMMER-III code. Their graphical representation is provided (together with the mass transfer models) in (Tobita et al., 2002).

Two models are available in the SIMMER-III code to represent the fuel pin: the simplified fuel pin model (SPIN) and the detailed fuel pin model (DPIN). ENEA has selected the SPIN model, while JRC has selected the DPIN model for the modelling and simulation of the CABRI-BI1 experiment and compared the results with ASTEC-Na and the real experiment.

2.3. SAS-SFR

The SAS-SFR code (Imke et al., 1994; JNES, 2011; Kruessmann et al., 2015) performs deterministic analysis for steady state power operation and accident conditions, caused by protected or unprotected loss of coolant flow or reactivity insertion in sodium-cooled fast reactors, during the so-called initiation phase. This code is the result of a long-term international cooperation between scientists from the KIT/INR (Germany), CEA, IRSN (France) and JAEA (Japan). The development started in the late eighties, taking as basis the SAS4A code developed at ANL (USA) for mixed-oxide fuel, where existing models have been improved and extended and new ones have been introduced.

SAS-SFR has been extensively qualified with a variety of results from various experiments. The test programmes covered a wide range of pin designs and test conditions such as: pre-irradiations from 0 to 12 at.% burnup, solid and hollow fuel pellets, transient power insertion starting at nominal cooling conditions up to extensive clad melting conditions with power transients from slow ramps (1% of nominal power per second) up to pulses with a half-width of a few ten milliseconds only.

[1] Non-equilibrium transfers are phase transition processes occurring at interfaces.
[2] Equilibrium transfers are phase transition processes occurring when a specific internal energy of a (bulk) component exceeds (or drops below) phase transition energy.

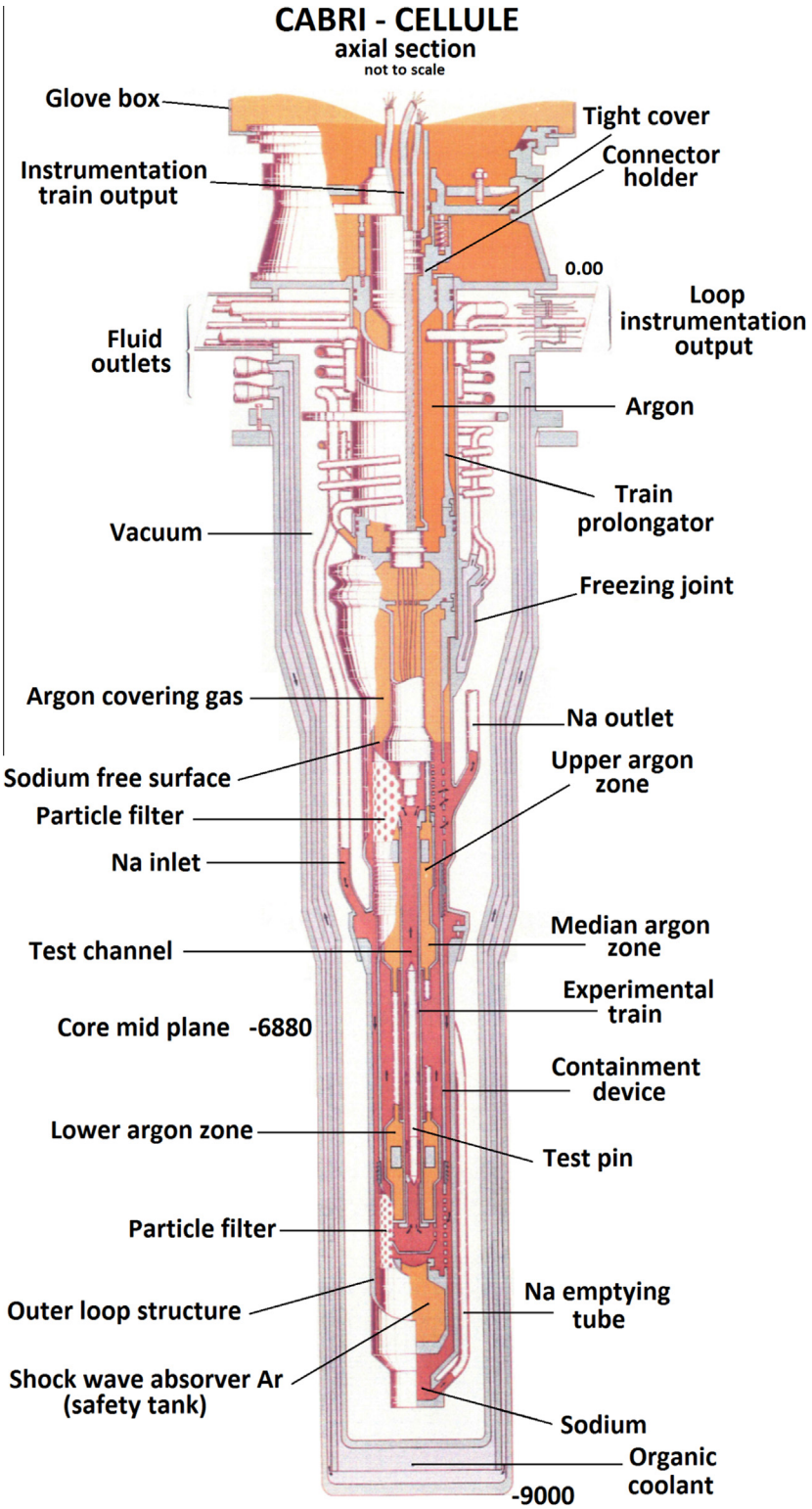

Fig. 1. Schematics of the CABRI reactor (CEA, 1989).

Major calculation models contained in SAS-SFR code include the steady state fuel irradiation behaviour, the transient fuel deformation behaviour, the primary main coolant system heat transport, the sodium boiling model, the cladding tube melting and motion analysis, the analysis of fuel failure behaviour in voided and unvoided regions.

The core nuclear and heat calculation model of SAS-SFR is a multi-channel model, grouping fuel assemblies with similar nuclear and heat characteristics into a channel which is represented by a single pin. The sodium voiding model is a multiple-bubble slug ejection model that handles flow area changes and non-uniform axial nodes. It simulates the rate and voiding extent for the voiding reactivity calculations, the heat removal from the cladding surface after the onset of voiding for the fuel and cladding temperature and the vapour flow rates that drive the cladding motion.

Table 1
Characteristics of RIG-1 fuel pins (Augier et al., 1981).

CLAD	
Outer diameter min/max [mm]	7.605
Inner diameter min/max [mm]	6.595
Material	316 – CW
PELLET	
Pellet diameter inner/outer [mm]	0/6.4
Fissile column length [mm]	748.8
Upper axial blanket length [mm]	99.5
Lower axial blanket length [mm]	200.2
Upper axial blanket pellets	Solid
Fissile pellet	Solid
Lower axial blanket pellet	Solid
Peak burnup [at.%]	1
PIN	
Pin length [mm]	1500.5
Effective upper fission gas plenum length [cm]	9.4

Table 2
Initial and boundary conditions for the CABRI BI1 experiment.

Physical parameter	Unit	Value
Power produced in the test section	W	37,120
Fissile power	W	36,230
Test channel inlet mass flow rate	kg/s	0.161 ± 3%
Temperature at BFC*	K	676 ± 0.3%
Temperature at TFC**	K	859 ± 0.3%
Sodium temperature increase	K	183 ± 0.53%
Sodium pressure at outlet	bar	2.43***
Sodium flow rate	kg/s	0.161

* BFC: Bottom of the Fissile Column.
** TFC: Top of the Fissile Column.
*** Experimental cover gas pressure.

The basic equation used in SAS-SFR to compute the mass flow and pressure drop is the following:

$$\frac{1}{A}\frac{dw}{dt}+\frac{dp}{dz}+\frac{1}{A}\frac{d(wv)}{dz}=-\left(\frac{dp}{dz}\right)_{fr}-\left(\frac{dp}{dz}\right)_{K}-\rho g$$

where the friction and orifice pressure drops and the gravity head are considered. Orifice coefficients are defined for upward and downward flows in order to compute the pressure drops along the simulated pin region in normal and abnormal operation. The equations from Bessiron (Bessiron, 1998) are used for the sodium equation of state.

The multiple bubble slug ejection model allows a finite number of bubbles separated by liquid slugs in a channel at any time. Voiding is assumed to result from formation of bubbles that fill the whole cross section of the coolant channel except for a liquid film left on cladding and structure surfaces. The liquid film around the vapour is assumed to be static. The vapour pressure is assumed to be uniform within small bubbles.

The module DEFORM-4C performs the fuel pin thermal-mechanics in SAS-SFR. The fuel-cladding gap conductance used is the standard URGAP-model which is the preferred one for experimental qualification of the DEFORM-4C model. It performs dynamic calculations at steady state and during transients considering not only the gap width, but also the inventory of initial gas and fission gases released and the contact pressure, respecting fuel and clad surface roughness, when the gap becomes closed.

3. Description of the CABRI experiment BI1

The CABRI facility was a pool-type research reactor originally devoted to studying the physical phenomena occurring in the course of an accident by observation of the behaviour of a single pin subjected to transient conditions in a highly instrumented test vehicle. One important feature of the CABRI facility was the hodoscope which allowed the observation of axial movement of the fuel during the tests by measuring the fission neutron emission during the experiments with a collimator array. CABRI consisted of a driver core in a swimming pool which supplied epithermal neutrons to the fast fuel pin located in a central loop with flowing sodium. The description of the test section is depicted in Fig. 1. It consisted on the test channel around the test pin, the instrumentation for controlling and observing the experiment and the structure that ensured the support of the test section and the safety of the test-loop under all temperature conditions.

For the BI1 test a pin from the CABRI RIG-1 irradiation in PHENIX reactor was used. The characteristics of these pins are presented in Table 1. Fissile and fertile fuel pellets in RIG-1 pins were full pellets (no as-fabricated central hollow). Fissile column was 75 cm high with 20 and 10 cm lower and upper blankets, respectively. There were both upper and lower fission gas plena.

The irradiation of RIG-1 lasted 64 days and a maximum burnup of 1 at.% was reached at the end of the irradiation.

The irradiated fuel pin was inserted into the CABRI test section and heated up to CABRI steady state conditions. Table 2 summarizes the initial and boundary conditions prior to the BI1 test.

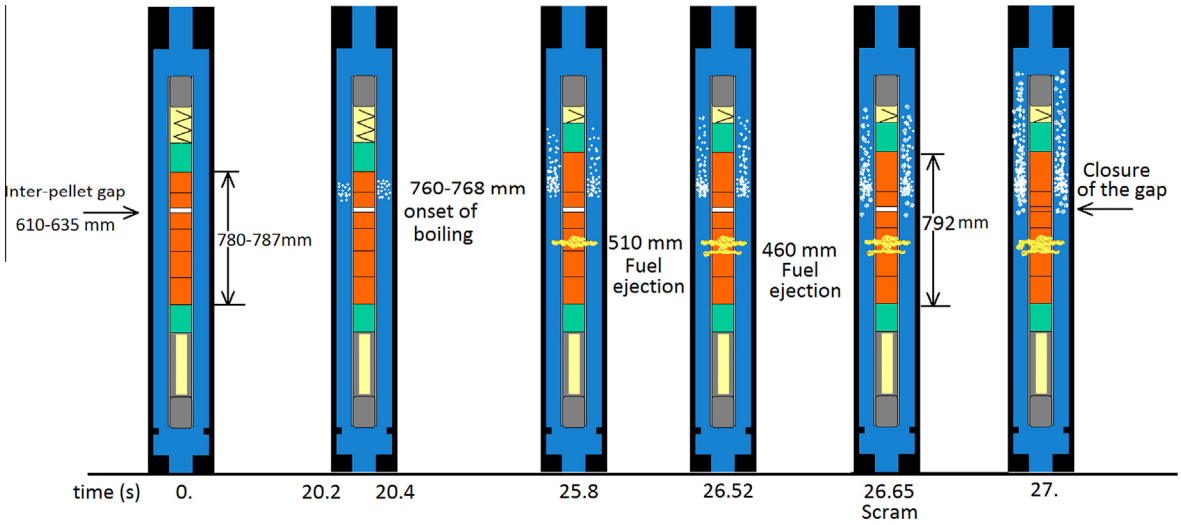

Fig. 2. Experiment evolution.

Table 3
ENEA (left) and JRC (right) model discretization for the BI1 test with ASTEC-Na.

Axial nodes	Section height (cm)	Radial		Axial nodes	Section height (cm)	Radial	
68	10	Sec. 5 Connection zone	Sec. 5 Connection zone	106	2	Sec. 6 Connection zone	
63–67	47.40	Sec. 4	By-pass	105	30	Sec. 5 Connection zone	Sec. 5 Connection zone
56–62	66.60	Sec. 3		104	47.50	Sec. 4	By-pass
54–55	12.73	Upper plenum		89–103	66.50	Sec. 3	
52–53	10	Top blanket		59–88	16.50	Upper plenum	
13–51	78.77	Fissile fuel		57–58	10	Top blanket	
9–12	20	Bottom blanket		18–56	78	Fissile fuel	
4–8	42.10	Lower plenum		14–17	20	Bottom blanket	
2–3	18.40	Sec. 2		4–13	42.10	Lower plenum	
1	1	Sec. 1 Connection zone		2–3	18.40	Sec. 2	
				1	10	Sec. 1 Connection zone	

Table 4
ENEA (left) and JRC (right) model discretization for the BI1 test with SIMMER-III.

Axial nodes	Section height (cm)	Radial			Axial nodes	Section height (cm)	Radial		
70	10	Connection zone			82	32	Connection zone		
65–69	47.50	Sec. 4	Virtual wall	By-pass	80–81	47.4	Sec. 5	Virtual wall	By-pass
58–64	66.50	Sec. 3			76–79	66.6	Sec. 4		
56–57	16.50	Upper plenum			74–75	16.5	Sec. 3		
54–55	10	Top blanket			72–73	8.069	Top blanket		
15–53	78	Fissile fuel			14–71	78.67	Fissile fuel		
11–14	20	Bottom blanket			10–13	20.07	Bottom blanket		
6–10	42.10	Lower plenum			5–9	33.90	Lower plenum		
5	4.6	Sec. 2			4	8.20	Sec. 2		
2–4	13.8	Sec. 1			2–3	18.40	Sec. 1		
1	5	Connection zone			1	10	Connection zone		

Table 5
Axial scheme used in SAS-SFR simulation of RIG-1 pin.

Axial nodes	Section height (cm)	Radial
39–40	47.4	Sec. 5
35–38	66.6	Sec. 4
33–34	16.5	Sec. 3
31–32	10	Top blanket
13–30	75	Fissile fuel
9–12	20	Bottom blanket
4–8	33.9	Plenum
3	8.2	Sec. 2
1–2	18.4	Sec. 1

The LOF transient was initiated by reducing the pump head of the test loop resulting in a reduction of the mass flow rate in the test section following approximately the equation (Augier et al., 1982):

$$\frac{Q}{Q_{t=0}} = \frac{1}{1+\frac{t}{\tau}} \quad \text{with } \tau = 7.5\text{–}8 \text{ s}$$

The reducing mass flow rate in the test section led to a temperature increase inside the test section channel, up to the onset of sodium boiling at the top of the active part of the fuel pin after $t = 20.2$ s. The phase change led to a sudden decrease of mass flow rate at the test section inlet. Then the boiling region rapidly extended towards the lower part of the fuel pin, while a fluctuating mass flow rates of the lower and upper coolant slugs established within the test section. Clad dry-out conditions were reached during the test leading to enhanced clad temperature increase up to its melting point. The clad melting extended above ~60 cm at the end of the transient phase. Some molten fuel escaping into the coolant channel of in total about 6 g was observed. Although the scram of the reactor occurred at $t = 26.65$ s after the onset of the transient, the sodium boiling phase and mass flow rate fluctuations continued after scram, until the regular mass flow rate was restored in the test section at approximately $t = 70$ s.

Fig. 2 shows a schematic view of the BI1 experiment evolution (blue represents the liquid sodium and white dots the sodium vapour). Particularities of the pin used for BI1 were several inter pellet gaps within the fissile height, which probably have occurred during several handling procedures moving the pin upside down during the time period between end of irradiation and insertion into the CABRI test section. The largest gap extends at steady state from 610 to 635 mm BFC.

4. Modelling

4.1. ASTEC-Na model

For benchmarking purposes ENEA and JRC have developed separate models of the BI1 test section by using ASTEC-Na v1.1p1. Table 3 shows the model discretization developed by ENEA and JRC. Full scale test section (from the lower plenum inlet up to the upper volume in contact with the cover gas) including bypass is represented in both models with only minor differences. The exit connection in the ENEA model is divided in two volumes (Section 5) one for the test section channel and another one for the bypass. The JRC model first is divided in two volumes (Section 5) one for the test section channel and another one for the bypass and after both are connected to a common volume (Section 6).

The irradiated fuel pin geometry data, represented in ASTEC-Na models were taken from (Augier et al., 1981).

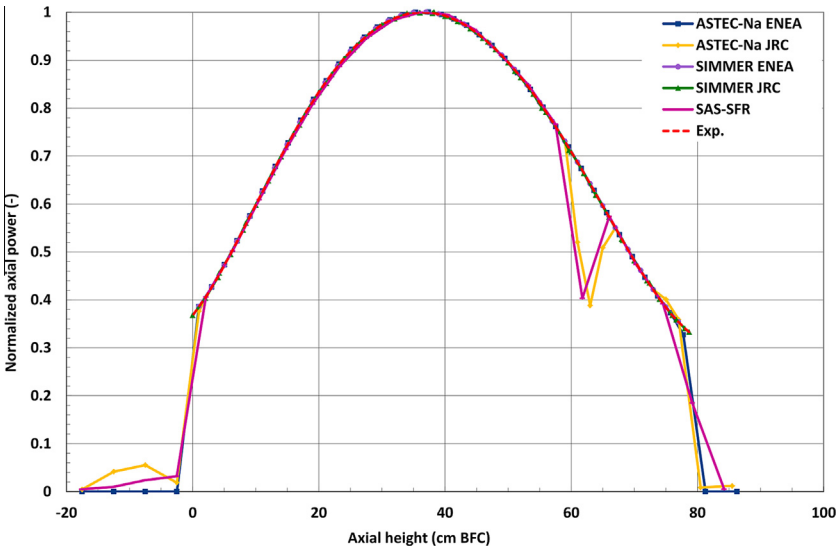

Fig. 3. Axial power profile used in the different calculations.

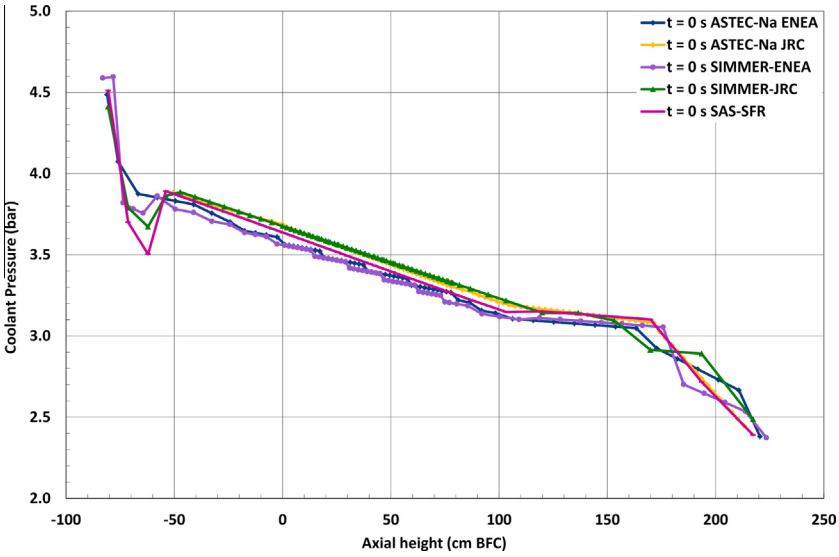

Fig. 4. Axial profile of the coolant pressure at steady state conditions for the different calculations.

The models were made using two ASTEC-Na modules – CESAR and ICARE. The lower plenum and the inlet channels of the test section and the bypass are represented by CESAR volumes and junctions, so as the upper plenum and the top volume in contact with the cover gas. The test section (including the fuel pin, the shroud, the insulation, the pressure tube and the channel walls) are represented by ICARE.

The thermal coupling between the inner test section channel and the outer bypass channel is simulated in actual geometry, in the axial region occupied by the fuel pin (active + fertile column), by representing the conductive radial heat exchanges through the different shroud layers and gaps: the inner niobium shroud, the xenon gap, the molybdenum–niobium shroud, the zirconia insulation and the zircaloy pressure tube.

In the ENEA calculation, heat losses from the thin wall above the fuel column are considered by imposing, as boundary condition, external temperature and heat exchange coefficient. Assumed values have been adjusted to roughly fit the results of SAS-SFR calculation.

The mass flow rate of sodium is imposed at the lower plenum inlet according to the total loop mass flow rate. The mass flow rate in the bypass channel is determined according to test specifications through a calibrated singular pressure drop coefficient inserted in the upper part of the bypass channel. The pressure at the upper volume outlet is imposed as constant during the whole transient, and according to the cover gas pressure in steady state conditions.

The main thermal–hydraulic data concerning the steady state conditions before the transient phase are summarized in Section 5.1. The initial conditions at the beginning of the transient phase (t = 0 s) are stabilized through a steady state calculation lasting 300 s, starting from an isothermal condition at zero power and then progressively increasing the fuel pin power up to the nominal value.

The calculated heat losses from the fuelled section of the test channel are ~130 W in good agreement with CABRI loop estimation.

Table 6
Steady state thermal characteristics.

Physical parameter	Unit	Experiment	ENEA		JRC		KIT
			ASTEC-Na	SIMMER	ASTEC-Na	SIMMER	SAS-SFR
Power produced in the test section	W	37120	37,120	37,120	36,510	37,120	36,844
Fissile Power	W	36230	37,120	37,120	36,510	37,120	35,738
Test channel inlet mass flow rate	kg/s	0.161 ± 3%	0.161	0.161	0.161	0.161	0.159
T_{inlet}	K	676 ± 0.3%	676.00	676.22	676.03	676.66	676.60
T_{outlet}	K	859 ± 0.3%	828.84	838.27	844.65	878.65	846.20
Temperature at BFC	K	677	675.91	676.21	676.15	676.29	677.50
Temperature at TFC	K	852–869	867.50	876.09	854.70	859.02	855.00
Sodium heat up along fissile height	K	183 ± 0.53%	191.59	199.88	178.55	182.73	169.60
Sodium pressure at BFC	bar		3.60	3.60	3.68	2.70	3.64
Sodium pressure at TFC	bar		3.20	3.20	3.30	2.40	3.27
Sodium pressure at outlet	bar	2.43*	2.38	2.38	2.39	2.39	2.39

* Experimental cover gas pressure.

Table 7
Physical characteristics of the fuel pin.

	ASTEC-Na ENEA	ASTEC-Na JRC	SIMMER ENEA	SIMMER JRC	SAS-SFR	Avg.	STD
Fuel clad gap width (μm)	0.000	10.005	15.000	9.750	0.000	6.951	6.682
Inner fuel radius (mm)	0.508	0.060	0.000	0.000	0.475	0.209	0.260
Outer fuel radius (mm)	3.349	3.311	3.283	3.200	3.333	3.295	0.059
Inner clad radius (mm)	3.306	3.321	3.298	3.298	3.333	3.311	0.016
Outer Clad Radius (mm)	3.813	3.826	3.803	3.803	3.838	3.816	0.015
PPN Axial Location (cm BFC)	37.365	37.000	37.000	36.000	36.180	36.709	0.588
Peak Linear Rating (W/cm)	638.704	638.670	641.320	626.908	621.100	633.340	8.832
Axial Height of the Fissile Column (cm)	78.770	78.000	78.000	78.670	76.647	78.017	0.847
Nodes in the fissile column	38	38	39	58	18	38.200	14.149

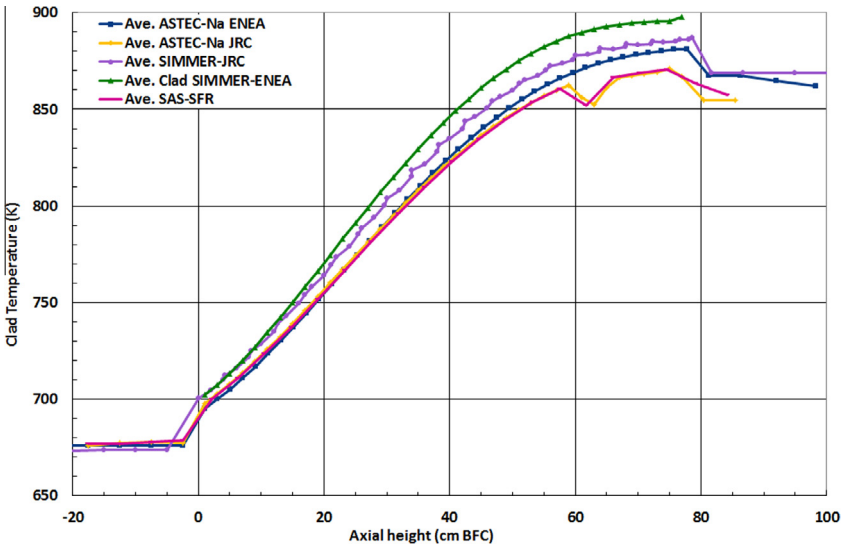

Fig. 5. Average clad temperature profiles at steady state conditions prior to BI1 transient.

4.2. SIMMER-III model

For the simulation of the BI1 experiment in SIMMER-III the detailed pin model (DPIN) was chosen by JRC, while the basic 2-node fuel pin model was used by ENEA. In the SIMMER-III simulation by JRC, 82 axial by 3 radial meshes and 7 internal nodes in the fuel pin were used. The first radial section was reserved for the test channel, the second radial section is a no-calculated zone and only the bottom and top parts are connected between the test channel and the bypass, the third radial section was reserved for the bypass region. In the SIMMER-III simulation by ENEA, 5 radial meshes and 70 axial meshes and 2 internals nodes in the fuel pin were used. The inner radial mesh was reserved for the test channel and the outer one for the bypass. The internal radial meshes were used to simulate heat losses from the test channel by fictitious loops filled with air and through calibrated convective heat exchanges. Table 4 shows the JRC and ENEA SIMMER-III models for the BI1 test.

4.3. SAS-SFR model

The axial meshing scheme used in SAS-SFR code for RIG-1 pin is presented in Table 5. For the fuel region 11 radial nodes and 24 axial nodes have been used. Lower and upper plena are simulated as only one plenum below fissile height with the gas volume of both plena.

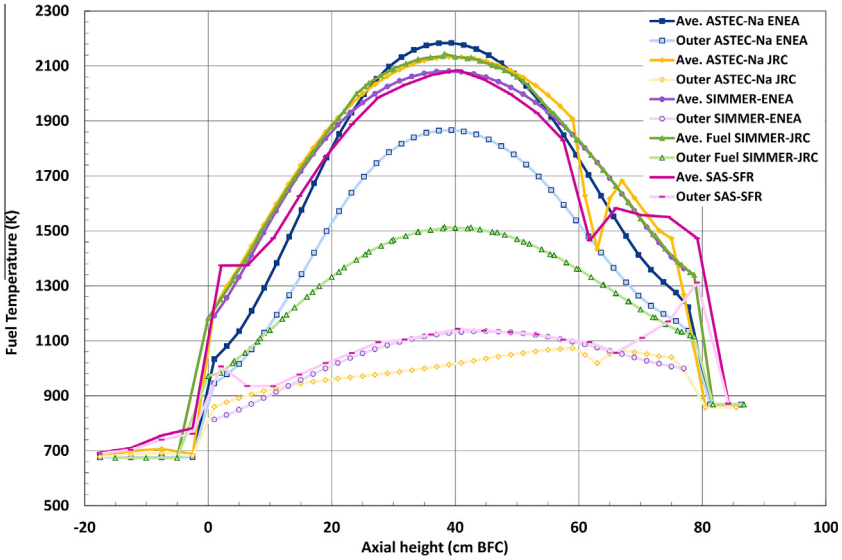

Fig. 6. Outer and average fuel temperature profiles at steady state conditions prior to BI1 transient.

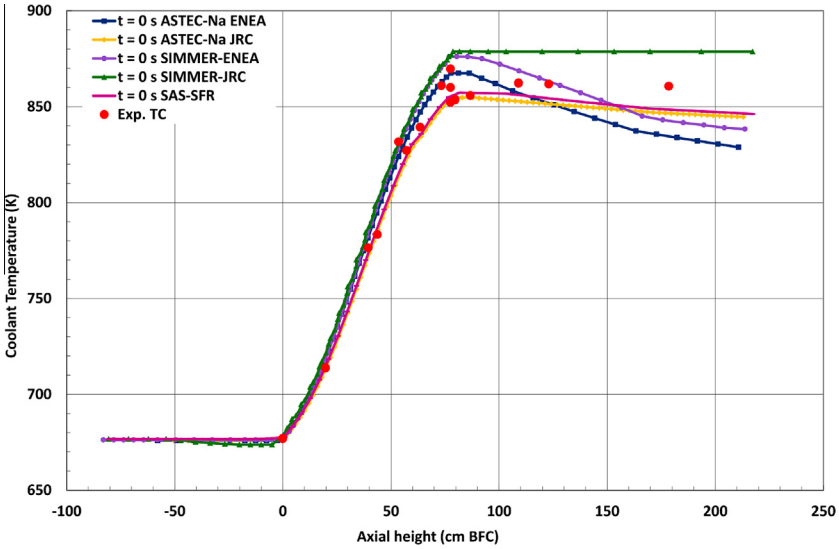

Fig. 7. Axial coolant temperature at $t = 0$ s.

For considering the axial pellet gap detected in BI1 pin, a power profile with a stepwise gap of power production is simulated at around 60 cm BFC (see Fig. 3)

The coolant inlet temperature, flow rate and outlet pressure are specified as a function of time in the input. Outlet pressure values are taken on the basis of experimental cover gas pressure measurements. Inlet pressure is calculated according to the pressure drops along the test section. Inlet and outlet flow rates after boiling are calculated by the multi-bubble model of SAS-SFR. Cooling cross sections along fuel height are adjusted transiently by SAS-SFR, whereas outside that region and also hydraulic diameters have been taken as constant neglecting the influence of spacers and support lines for instrumentation. These last elements are considered to have only a small effect on experimental results and are in this aspect not decisive for the transient simulation.

The coolant bypass is not simulated in SAS-SFR code, only the test section is modelled from test section coolant inlet up to coolant outlet including the cover gas plenum of the test section. Since the test section flow path is connected to a separate cover gas plenum which has no direct connection to the bypass flow path, the test section plena have considerably different pressures than respective positions of the bypass flow path. This fact is important in the simulation because during the LOF transient the bypass flow hardly intervenes with the dynamics of the two-phase flow. Therefore modelling of the bypass flow is not necessary for the simulation of the test.

The radiation heat losses through the xenon gap in the insulation/protection structure around the test channel are simulated according to qualification exercises performed for the LOF and LOF + TOP[3] CABRI experiments using the same test section design. Considering radial heat losses is particularly important in this BI1 transient with extended boiling time period, because the axial coolant temperature distribution within and above the fissile height affects the transient boiling behaviour through condensation and vaporization.

[3] TOP: Transient Over Power.

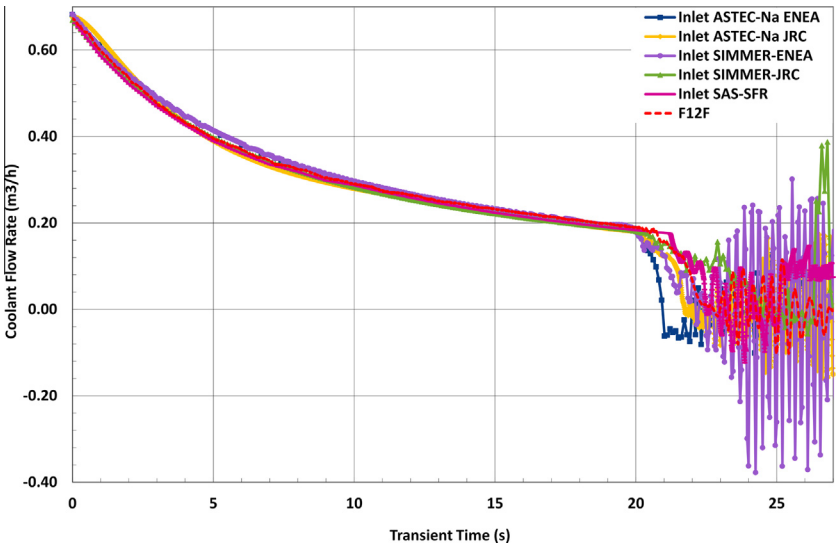

Fig. 8. Inlet flow rate during the first 27 s of the transient.

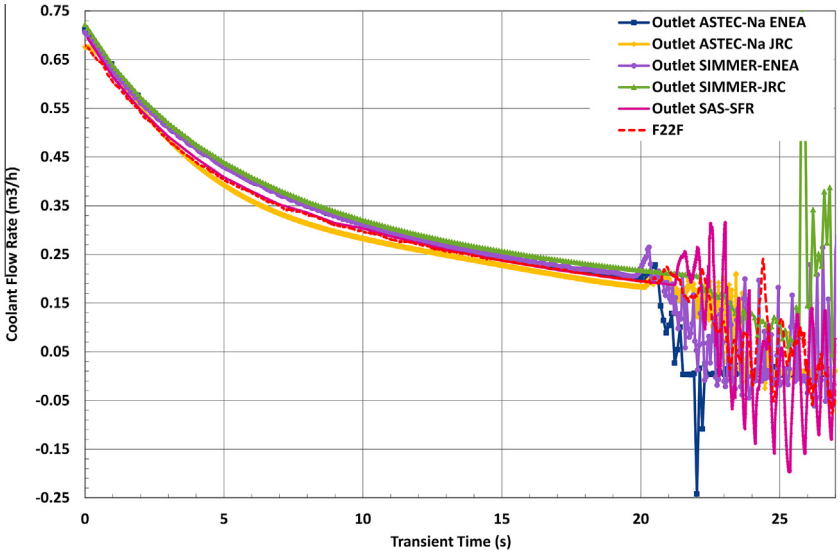

Fig. 9. Outlet flow rate during the first 27 s of the transient.

5. Simulation and comparison codes-experiment

5.1. Steady state

The main goal of the steady state calculations is to replicate the experimental state before the beginning of the transient as precise as possible.

In the experiment, initially the fuel pin is cooled by a mass flow rate which amounts to 0.161 kg/s, entering the test section at a temperature of 676.8 K, reaching at top of fissile column a temperature of 853.3 K, experiencing a temperature increase of 176.5 K. The total fission power is 35267.0 W.

For considering the axial pellet gap detected in BI1 pin, ASTEC-Na JRC and SAS-SFR have used the power profile plotted in Fig. 3, where a stepwise gap of power production is simulated at around 60 cm BFC.

The axial pellet gap was not considered in the SIMMER-JRC, SIMMER-ENEA and ASTEC-Na ENEA calculations.

The Fig. 4 shows the axial profile of the coolant pressure in steady state for the different calculations.

The inlet mass flow rate of sodium is imposed in the calculation according to the total loop mass flow rate. For the codes simulating the bypass, the mass flow rate in the bypass channel is determined according to test specifications through a calibrated singular pressure drop coefficient inserted in the upper part of the bypass channel. Outlet pressure is imposed as well in all calculations according to the cover gas pressure measurements.

The main thermal–hydraulic and power data concerning the steady state conditions are summarized in Table 6. The simulation of the steady state conditions is achieved starting from an isothermal condition at zero power and then progressively increasing the fuel pin power up to the nominal value.

Table 7 shows the physical fuel pin characteristics that were achieved at the end of steady state simulation.

In Fig. 5 it can be seen the influence of the inter pellet gap on the calculated average clad temperatures for the models of ASTEC-Na JRC and SAS-SFR.

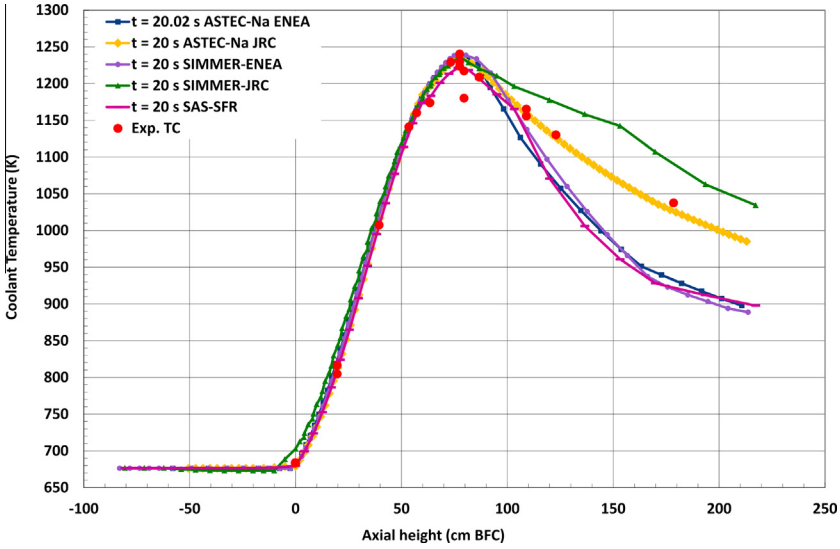

Fig. 10. Axial coolant temperature at $t = 20$ s.

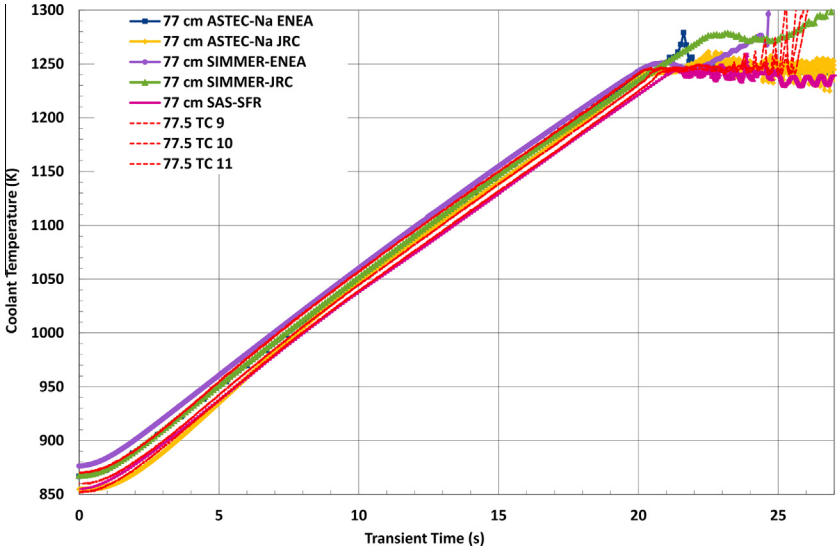

Fig. 11. Coolant temperature evolution at 77 cm BFC during the LOF transient.

ASTEC-Na ENEA calculation predicts much higher outer fuel temperature than the ASTEC-Na-JRC calculation (see Fig. 6). This is mainly due to the rough radial meshing adopted in the ASTEC-Na ENEA model.

At the beginning of the transient the calculated coolant temperature values well match the experimental data (Exp. TC) at the inlet and fissile region (see Fig. 7); the calculation by SIMMER-JRC keeps the coolant temperature constant above the fissile region and the ASTEC-Na ENEA calculation decrease faster than the experimental data. The calculations with ASTEC-Na JRC and SAS-SFR are the closest to the experimental data.

5.2. Transient

5.2.1. Inlet/outlet flow rate

The time evolution of the mass flow rate at the test section inlet is shown in Fig. 8 (inlet) and Fig. 9 (outlet) where they are compared to the inlet and outlet flowmeters (F12F and F22F, respectively).

The onset of boiling and the mass flow rate oscillations during the boiling phase inside the test section channel starts around 20 s as shown in Fig. 8 (inlet) and Fig. 9 (outlet). The mass flow rate decrease at the onset of boiling is more pronounced in the calculation by ASTEC-Na ENEA, SIMMER-ENEA and ASTEC-Na JRC; the calculations by SIMMER-JRC agree better at the beginning of the boiling until 22 s into the transient. SAS-SFR follows rather close to the behaviour of the experimental data. Discrepancies with the experimental measurements depend, at least in part, on different input models, because same codes (ASTEC-Na and SIMMER III) predict different behaviours depending on the user (ENEA or JRC).

For the outlet flow rate (see Fig. 9) it seems as if the oscillations calculated by SIMMER-ENEA, ASTEC-Na JRC, ASTEC-NA ENEA and SAS-SFR are inside of the region of amplitude of the experiment (-0.15 to 0.25 m^3/h) with some peaks outside of this region and at about 26 s the SIMMER-JRC predicted a high peak in the outlet flow rate.

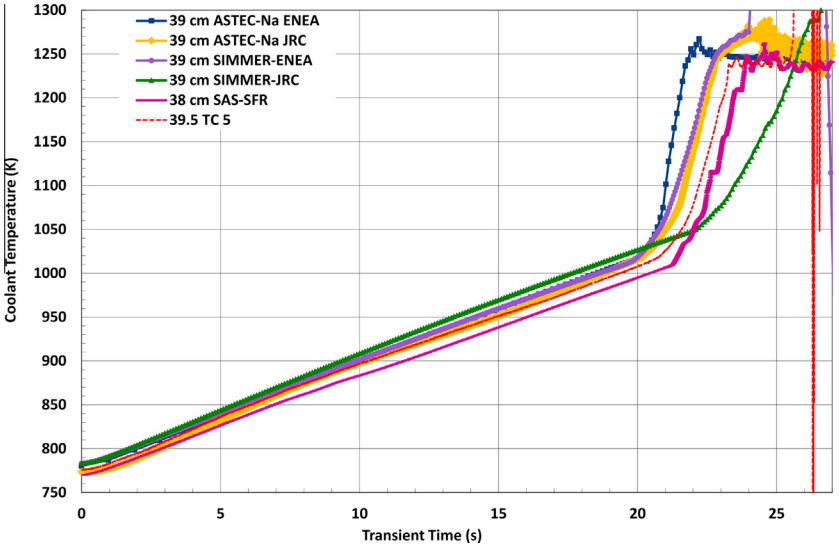

Fig. 12. Coolant temperature evolution at ~39 cm BFC during the LOF transient.

5.2.1.1. Coolant temperature. The axial sodium temperature profile is compared to thermocouple measurements just before the onset of boiling (t = 20 s Fig. 10). The calculations follow very well the experimental data in the lower region and through the fissile fuel column. In the upper region the temperature decrease differs except for ASTEC-Na JRC. SAS-SFR, SIMMER-ENEA and ASTEC-Na ENEA predict a lower temperature while the calculation by SIMMER-JRC overestimates the coolant temperature. The calculation by ASTEC-Na JRC follows correctly the experimental data (Exp. TC).

Again the discrepancies depend on the model, at least for the SIMMER-III and ASTEC-Na, because two partners are using the same codes. In particular, the temperatures above the fuelled region depend on radial heat losses assumptions.

The evolution of coolant temperatures at different axial fuel pin heights above the BFC are plotted in Figs. 11–13.

The sudden increase in coolant temperature after onset of boiling and consequent stop of mass flow rate at the test section inlet is rather well captured by the codes at all elevations.

The calculated coolant heat-up rate at the boiling onset is well correlated with the flow rate decrease, again at the boiling onset (Fig. 8). Maximum and minimum heat-up rate are calculated respectively by ASTEC-Na-ENEA which exhibits the more pronounced flow rate decrease and SIMMER-JRC that predicts a very slow decrease of flow rate.

The codes also predict the onset of boiling at various elevations, around 20–25 s, that is the time at which the coolant temperature reaches the saturation value.

The high pin bending in BI1 pin affected all events in the channel. This can be observed in the thermocouple measurements presented in Fig. 11. The three thermocouples are located at the same axial height, but there are considerable differences in the measurements in the three azimuthal locations. Codes predictions are roughly inside the observed measurements dispersion.

Near saturation temperature, before permanent clad dry-out, clad undergoes rewetting which is the combination of coolant flow rate oscillations at the high linear power rating of the BI1 experiment. These rewetting sequences can be observed in Fig. 14 as

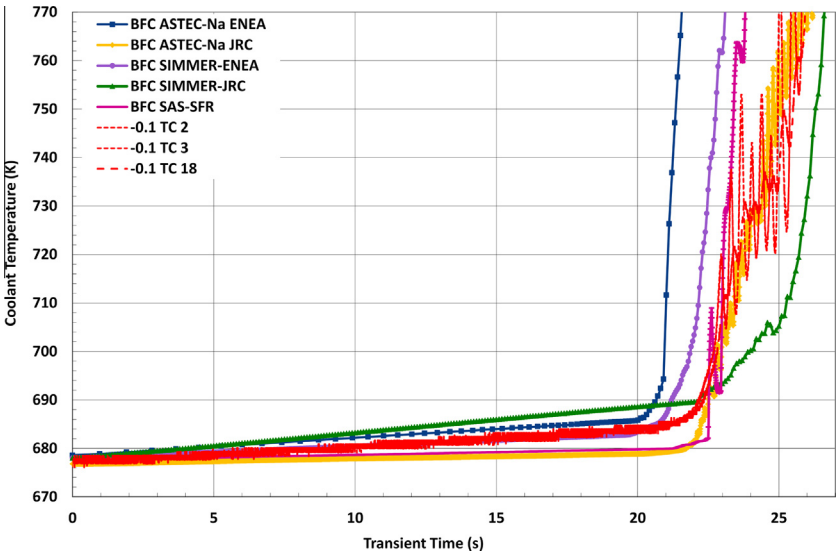

Fig. 13. Coolant temperature evolution at BFC during the LOF transient.

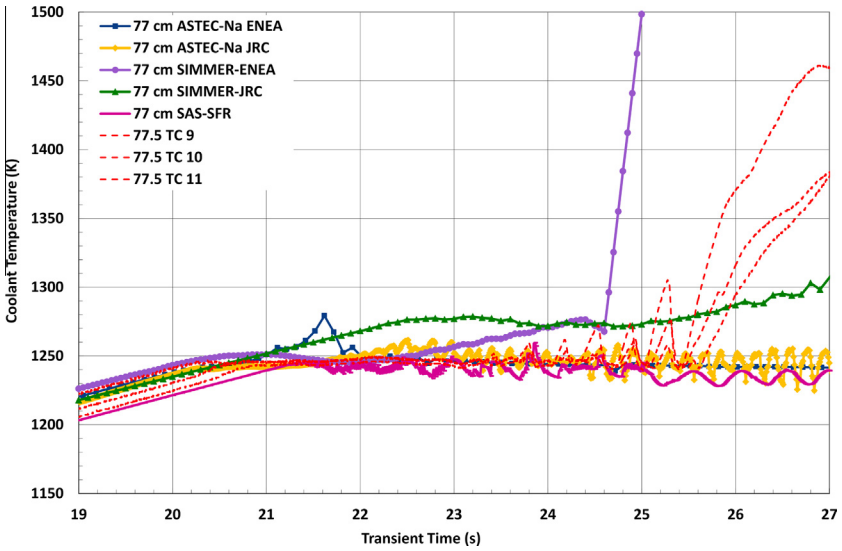

Fig. 14. Coolant temperature behaviour near saturation temperature at 77 cm BFC.

small peaks around the saturation temperatures. After dry-out, thermocouples are exposed to radiation heat transfer from overheated clad surfaces and the transient measurements are not valid anymore but only representative for the local coolant temperature variation.

5.2.1.2. Pressure. Outlet pressure is imposed in the calculations for the single phase on the basis of the cover gas pressure measurements. Inlet pressure is then computed according to the calculated pressure drop along the test section. The coolant pressure follows the flow rate decrease (Fig. 15). After 20 s small oscillations start to appear in the pressure due to boiling of the sodium (Fig. 16), the pressure calculation by SIMMER-JRC increases after around 15 s (Fig. 16).

For the bottom and top fuel small pressure decrease was detected for the SIMMER-ENEA around 5 s (see Fig. 15).

5.2.1.3. Sodium two-phase interphase. The sodium two-phase interface locations are plotted in Fig. 17. Red dots represent experimental measurements of thermocouples reaching saturation temperature and void detector measurements. There are some differences among the measurements of the various thermocouples.

As it can be seen in Section 4.1, the upper plenum zone modelled by ASTEC-Na JRC has a finer mesh compared with the other models. ASTEC-Na JRC used 30 axial nodes to modelling this section and the other models only used 2 axial nodes.

The fine mesh in the upper plenum used by ASTEC-Na JRC improves the calculations of the boiling front propagation compared to the other ASTEC-Na results from ENEA as can be seen in Fig. 17. The upwards front is underestimated by ASTEC-Na ENEA calculation and overestimated by ASTEC-Na JRC. For ENEA results the discrepancy is due, at least in part, to an overestimation of heat losses above the fuelled region that enhance sodium vapour condensation. The hypothesis is supported by the underestimation of temperatures (Figs. 7 and 10) in the same region. Sensitivity studies also showed an important effect of the axial meshing on the evolution of boiling fronts.

5.2.2. Comparison of main events

The calculation by SIMMER-JRC reaches the boiling onset earliest than the other codes and SAS-SFR reaches this even latest than

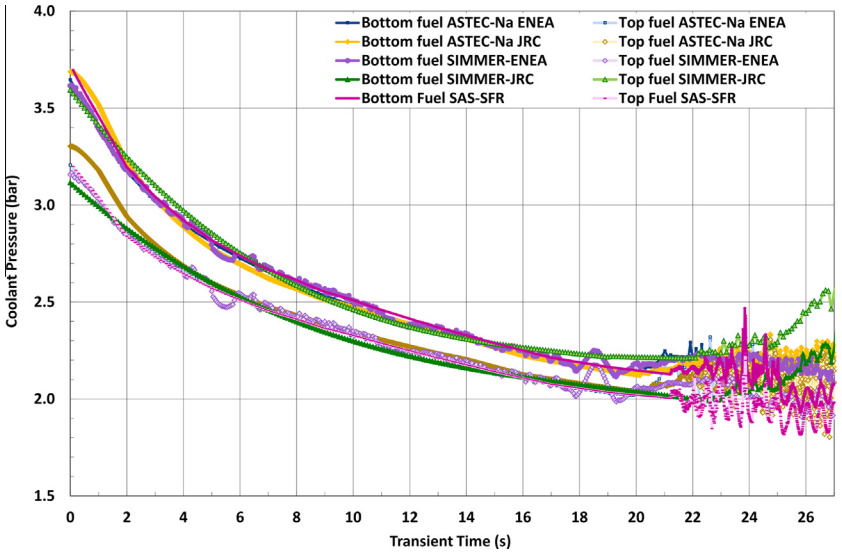

Fig. 15. Coolant pressure evolution at bottom and top of the fuel column (from 0 to 27 s).

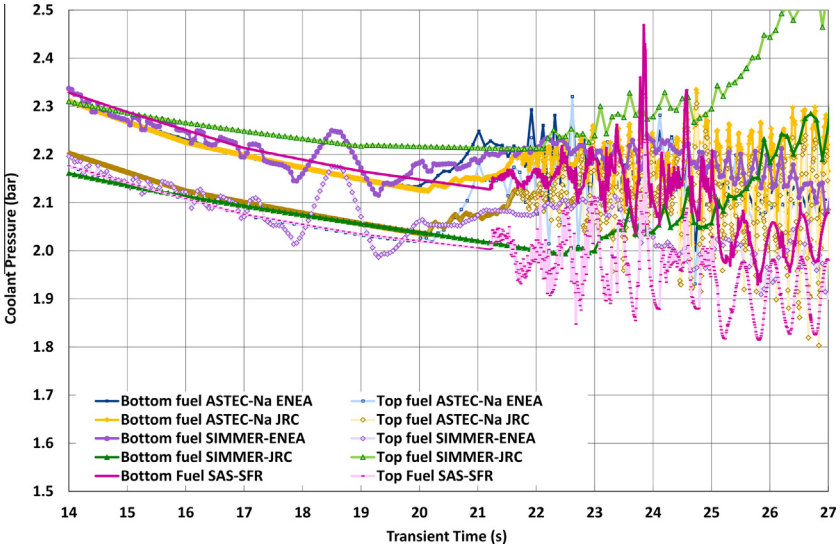

Fig. 16. Coolant pressure evolution at bottom and Top of the fuel column (from 14 to 27 s).

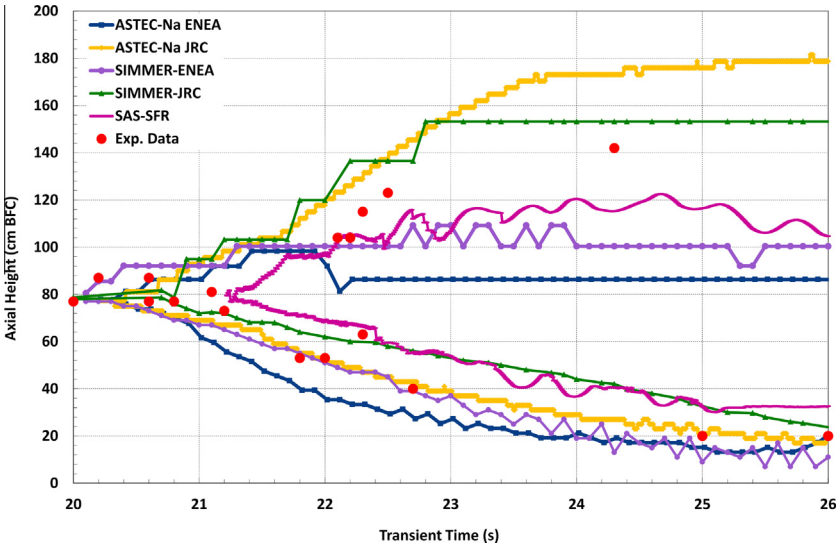

Fig. 17. Sodium two-phase interface during BI1 test.

Table 8
Main events.

Event	Exp. (Augier et al., 1981)	ASTEC-Na ENEA	ASTEC-Na JRC	SIMMER-JRC	SIMMER-ENEA	SAS-SFR
Boiling onset time (s)	20.2–20.8	20.1	20.2	19.9	20.1	21.2
Boiling onset height (cm BFC)	76.8	77.8	77.0	78.7	77.0	79.6
Saturation temperature (K)	1244.0	1240.0	1240.0	1233.2	1243.2	1242.5
Clad melt through (liquidus) time (s)	24.2–24.9	~23	24.1	25.3	24.1	24.4
Clad melted at scram (cm BFC)	16–76.8	12.1–78.8	30.0–78.7	29.7–78.7	26.0–78.0	20.7–76.6
Fuel melting	25.8 s at 51 cm BFC first ejection*	23.4 s at 39.4 cm BFC	24.9 s at 39.4 cm BFC	25.9 s at 46 cm BFC	25.9 s at 42 cm BFC	20.0 s at 40.6 cm BFC
CPU time calculation(s) for 27 s of simulation		8.34824E+02	9.38000E+02	1.44762E+05	1.72000E+04	4.50000E+01
Hardware specifications		Intel core i5-2410 M CPU 2.3 GHz 4 GB RAM	Intel core i7-3770 CPU 3.4 GHz 16 Gb RAM	2× Intel Xeon E5-2640 CPU 2.5 GHz 128 GB RAM**	Intel core i7 2600 K CPU 3.4 16 GB RAM	16 Intel Xeon E5620 CPU 2.4 GHz 24 GB RAM**

* Fuel ejection through the clad break-up but not fuel melting onset.
** Memory shared with other calculations.

the other codes. The height of boiling onset is found in all calculations at the Top of the Fissile Column (TFC). The differences with the experimental value come from the length of the nodes considered. Fuel melting onset is reached at different transient times according to the various calculations. ASTEC-Na ENEA predicts 23.4 s at 39.4 cm while the other ASTEC-Na calculation by JRC predicts 24.9 s at 39.4 cm. SAS–SFR predicts fuel melting onset at 20.0 s while for SIMMER it is reached at 25.9 s.

The Table 8 summarize the calculations results.

6. Conclusions

In this paper five different models from three different institutions, ENEA, JRC and KIT using three different codes, SAS-SFR, ASTEC-Na and SIMMER-III were presented. Despite of some small differences the calculations are generally in good agreement with the experimental data.

The BI1 test has two important peculiarities. One is a significant axial inter pellet gap detected in the fissile column and the other is the high pin radial bending occurring during single phase coolant heat-up considerably prior to boiling onset. These two facts lead to a complex task when trying to simulate the experiment with whatever code.

The SAS-SFR and ASTEC-Na JRC models took into account the inter-pellet gap, the effects of the inter pellet gap are mainly seen in the fuel temperature.

The latest boiling onset time was calculated by SAS-SFR (21.20 s) and the earliest by SIMMER-JRC(19.90), the average time for all the calculations (20.3 s) is inside of the experimental interval time between local and bulk boiling onset (20.2–20.8 s).

The models of ASTEC-Na, ENEA and JRC, reached the boiling onset time in 20.12 and 20.18 s, respectively. Both calculations are inside of the experimental interval time.

The coolant axial profile calculated by ASTEC-Na JRC at 20 s, fit almost perfectly with the experimental data (see Fig. 10).

All the calculations have a good agreement with the two-phase front downwards (see Fig. 17) the simulation by SIMMER-JRC is a little bit out of the average predicted by the other models and for the two-phase front upwards the models represent the experimental data worse, the calculation by ASTEC-Na ENEA is lower than the experimental data and the calculation by ASTEC-Na JRC predicts a higher value than the experimental data. Using the same code, both models predict totally opposite results, this is due, at least in part, to user assumptions on heat losses above the fuelled region.

Acknowledgement

This work was financed by the JASMIN project N°295803 within the 7th Framework Programme of the European Commission in the Topic Fission-2011-2.2.1 “Support for ESNII”. Special thanks to Dr. Dankward Struwe for the technical support provided during the preparation of this work on behalf of the KIT contribution.

References

Augier, G., Mitsuki, S., et al., 1982. CABRI TEST BI1 – Preliminary Report. IRSN, Cadarache.

Augier, G., Rongier, P., et al., 1981. Detailed Experimental Program of CABRI TEST BI1. IRSN, Cadarache.

Bessiron, V., 1998. Implementation of New Sodium Equations of State in SAS 4A, Note Technique SEMAR 98/26 IPSN.

Brillant, G., Laborde, L., 2014. Sodium Thermalhydraulics in ASTEC/CESAR. Confidential Rapport n. PSN-RES/SAG/2014-00008.

CEA, 1989. CABRI Project 1973–1988: Test Facility, Results and Achievements, Technical Note CEA/IPSN/DERS n° 01/89.

Chatelard, P., Reinke, N., et al., 2014. ASTEC V2 severe accident integral code main features, current V2.0 modelling status, perspectives. Nucl. Eng. Des. 272, 119–135.

Girault, N., Van Dorsselaere, J.P., et al., 2013. The European Jasmin Project for the Development of a New Safety Simulation Code, ASTEC-Na, for Na-cooled Fast Neutron Reactors. In: 2013 International Congress on Advances in Nuclear Power Plants & 28th KAIF/KNS Annual Conference, Jeju Island, Korea.

Imke, U., Struwe, D., et al. (1994). Status of the SAS4A-code development for consequence analysis of core disruptive accidents. In: Intl. Topic. Mtg. on Sodium Cooled Fast Reactor Safety, FRS'94, Obninsk, Russia.

JNES, 2011. A SAS4A Study on the ULOF Initiating Phase Energetics of the Fast Breeder Reactor (FBR). Japan Nuclear Energy Safety Organization.

Kruessmann, R., Ponomarev, A., et al., 2015. Assessment of SFR reactor safety issues: part II: analysis results of ULOF transients imposed on a variety of different innovative core designs with SAS-SFR. Nucl. Eng. Des. 285, 263–283.

Papin, J., 2012. 2.24 – behavior of fast reactor fuel during transient and accident conditions A2 – konings. In: Rudy, J.M. (Ed.), Comprehensive Nuclear Materials. Elsevier, Oxford, pp. 609–634.

Tobita, Y., Kondo, S., et al., 2002. The Development of SIMMER-III, An Advanced Computer Program for LMFR Safety Analysis, and Its Application to Sodium Experiments. Technical Meeting on the Use of Computational Fluid Dynamics Codes for Safety Analysis of Reactor Systems (Including Containment). IAEA/NEA, Pisa.